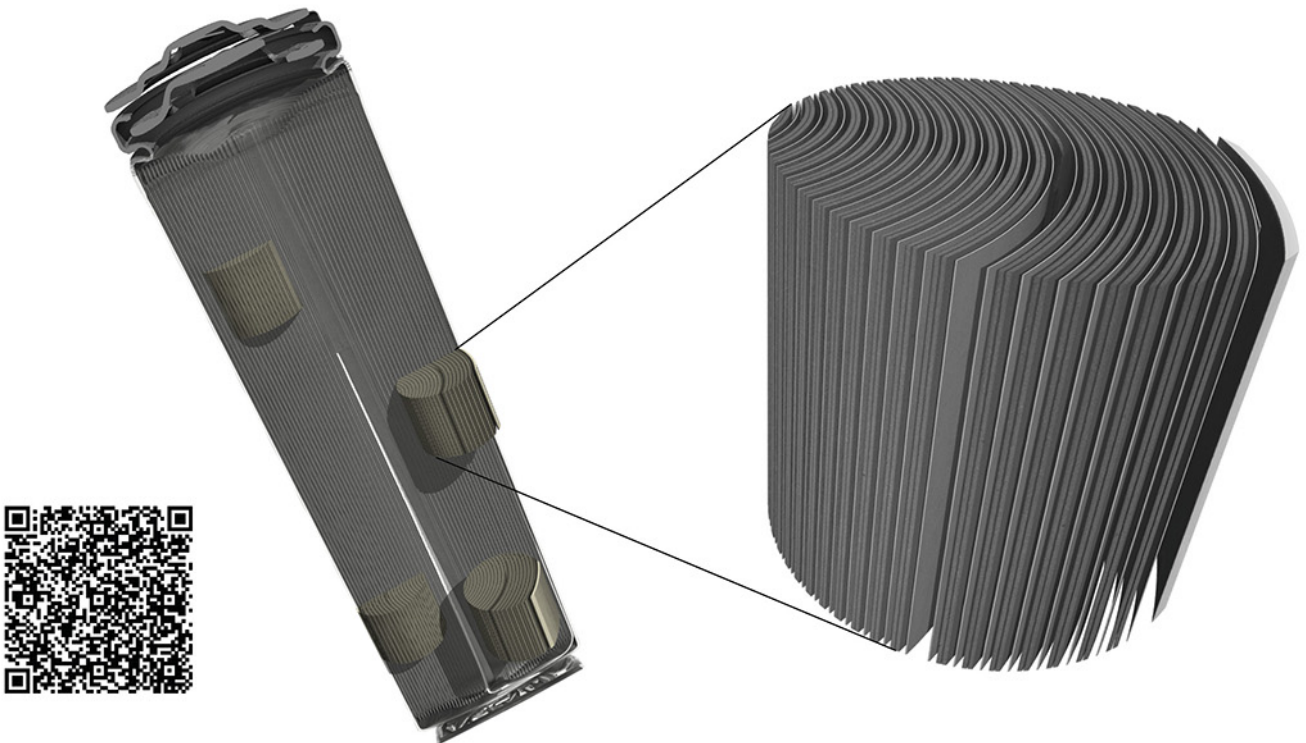


TESCAN micro-CT solutions

for energy storage materials research



TESCAN UniTOM XL

- ✓ Multi-scale non-destructive 3D imaging optimized to maximize throughput and contrast
- ✓ Fast scanning and high sample throughput with temporal resolutions below 10 seconds
- ✓ Wide array of samples types
- ✓ Enables dynamic tomography and *in-situ* experiments
- ✓ Dynamic screening for synchrotron beamtime
- ✓ Modular and open system with unmatched flexibility for research



[Click and find out more](#)

Improved Output Performance of Triboelectric Nanogenerator by Fast Accumulation Process of Surface Charges

Yanhong Li, Zhihao Zhao, Lu Liu, Linglin Zhou, Di Liu, Shaoxin Li, Shengyang Chen, Yejing Dai,* Jie Wang,* and Zhong Lin Wang*

As a promising energy harvesters, triboelectric nanogenerators (TENG) can be utilized to convert distributed energy into electric power, but the slow charge accumulation incorporated with the inevitable charge decay/leakage of conventional TENGs result in a low surface charge density and an inferior output performance, limiting their practical applications. Here, an effective strategy is proposed to realize high charge density by using a fast charge accumulation process on dielectric material with high relative permittivity. As a result, the charge density is tremendously improved to 2.20 mC m^{-2} on the poly(vinylidene fluoride-trifluoroethylene) film. Meanwhile, the fast charge accumulation is highly conducive to reach a high charge density of 1.30 mC m^{-2} in a 90% relative humidity environment, which is ≈ 260 times that of a TENG with slow charge accumulation. This work not only provides a new insight into charge accumulation and equilibrium state, but also provides significant guidance on the performance optimization of TENG.

1. Introduction

The past few decades have witnessed the rapid progress of portable electronic devices and wireless sensor networks, during which extensive efforts have been devoted to the development of mobile and distributed energy. The big data and the imminent era of the Internet of things promote the research of harvesting micro/nano energy and sustainable energy.^[1] In recent years, triboelectric nanogenerator (TENG) proposed by Wang's group,^[2] which can convert various environmental mechanical energy into electrical energy based on the coupling of triboelectrification effect and electrostatic induction effect, has attracted widespread attention.^[3–9] Taking advantage of low cost, wide selection of materials, simple preparation, light weight, and high pulsed

power density, TENG has been widely used in micro/nano-power sources, self-powered sensors, high-voltage source, and blue energy.^[10–19]

As an energy harvester, the wide range applications and commercialization of TENG are determined by its power density, which is quadratically related to its surface charge density.^[20] Generally, part of the surface charges will be consumed by the widespread existence of leakage current in dielectric film^[21] and air breakdown effect.^[22,23] The common TENG will quickly reach a low equilibrium state between the charge accumulation and charge decay (**Figure 1a (i)**) due to the inevitable degradations and limited surface charges generated by triboelectrification, accompanied by a low output performance.^[20,24] To increase the charge density, some efforts, e.g., high vacuum environment^[25] and high-pressure gas environment,^[26] have been devoted to suppressing the surface charge decay by avoiding air breakdown in a high surface charge density state (**Figure 1a (i)**). These strategies can significantly maintain high surface charge density as well as high output performance. However, the extreme environmental conditions are difficult to realize in practical applications.

On the other hand, there are some effective methods that can be utilized to increase the surface charges through enhancing the charge accumulation process. Taking advantage of ion injection,^[22] charge pumping,^[27,28] and external/self-charge

Y. Li, Dr. Z. Zhao, L. Liu, Dr. L. Zhou, D. Liu, S. Li, S. Chen, Prof. J. Wang, Prof. Z. L. Wang
Beijing Institute of Nanoenergy and Nanosystems
Chinese Academy of Sciences
Beijing 100083, P. R. China
E-mail: wangjie@binn.cas.cn; zhong.wang@mse.gatech.edu

Y. Li, S. Chen, Prof. J. Wang
School of Chemistry and Chemical Engineering
Center on Nanoenergy Research
Guangxi University
Nanning 530004, P. R. China

Dr. Z. Zhao, Dr. Y. Dai
School of Materials
Sun Yat-sen University
Guangzhou 510275, P. R. China
E-mail: daiyj8@mail.sysu.edu.cn

L. Liu, Dr. L. Zhou, D. Liu, S. Li, Prof. J. Wang, Prof. Z. L. Wang
College of Nanoscience and Technology
University of Chinese Academy of Sciences
Beijing 100049, P. R. China

Prof. Z. L. Wang
School of Materials Science and Engineering
Georgia Institute of Technology
Atlanta, GA 30332, USA

 The ORCID identification number(s) for the author(s) of this article can be found under <https://doi.org/10.1002/aenm.202100050>.

DOI: 10.1002/aenm.202100050

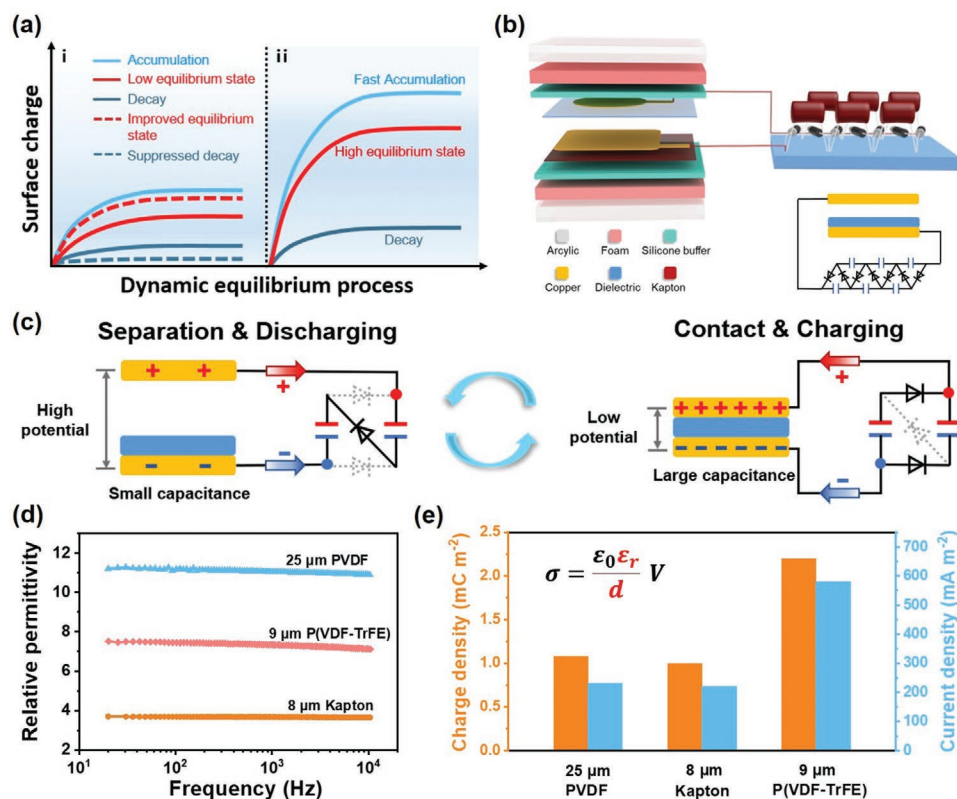


Figure 1. High equilibrium state and working mechanism. a) Schematic diagram of charge accumulation, charge decay, and dynamic equilibrium process. b) Structural illustration of self-charge excitation TENG in this work. c) Working mechanism of self-charge excitation TENG during periodic contact-separation process. d) Relative permittivity of three different dielectric layers. e) Surface charge density and output current density with three different dielectric layers.

excitation strategies,^[29,30] the charge accumulation speed can be effectively quickened. Despite the increased charge decay under high charge density,^[24] the surface charges will reach a higher equilibrium state due to the fast charge accumulation (Figure 1a (ii)), resulting in a higher output performance of TENG. Especially, the self-charge excitation circuit can increase the surface charges of TENG exponentially, which is an effective technology for breaking through the limitation of triboelectrification to realize high surface charge density. Therefore, it can be utilized to improve the equilibrium state of surface charges for further facilitating the development of high-performance TENG. However, the current researches mainly focus on polypropylene,^[28] polyimide,^[29] or polyetherimide (PEI) dielectric films,^[30] whose low relative permittivity requires the utilization of ultrathin dielectric layer to achieve a higher theoretical charge density.^[31] The latter will result in the decrease of contact efficiency^[30] or the increase of inner leakage current,^[21] limiting further improvements of output performance.

In this work, we propose an effective strategy to realize high charge density of TENG by using a fast charge accumulation process on dielectric material with high relative permittivity. Taking advantage of self-charge excitation and high dielectric permittivity of P(VDF-TrFE) film, the charge density of TENG can be enhanced to 2.20 mC m⁻². Meanwhile, the contact efficiency is increased to 82% by avoiding the utilization of

ultrathin dielectric layer. What is more, with the help of the fast charge accumulation, the high equilibrium state of surface charges is also realized in humidity environment, which is conducive to stable output performance under extreme conditions. Even at 90% relative humidity environment, the charge density can maintain at 1.30 mC m⁻², almost 260 times that of the common TENG. This work not only provides a new insight into the charge accumulation process and equilibrium state, but also has a crucial guiding significance for optimizing the output performance of TENG.

2. Results and Discussion

2.1. Fast Charge Accumulation and High Equilibrium State

The structure of TENG with fast charge accumulation is shown in Figure 1b (the inset is the corresponding circuit diagram). To better understand the charge accumulation and charge transferring processes, one voltage multiplier circuit (VMC) unit is taken as an example for illustration, which is composed of two capacitors and three rectifier diodes, as shown in Figure 1c. During the periodic contact-separation movements of TENG, the external capacitors can be switched between series-connected and parallel-connected automatically, resulting in alternate charging and discharging to realize charge

accumulation. When the two friction layers are separated, the external capacitor group is switched to the series-connected. Meanwhile, the capacitance of TENG decreases significantly while voltage increases sharply, leading to the transfer of charges from TENG to the external capacitors. On the contrary, in the contact process of TENG, the external capacitors are automatically switched to the parallel-connected due to the unidirectional conductivity of diodes. At the same time, the capacitance of TENG increases while the voltage decreases, so the charges in the external capacitors are fed back to TENG until the potential difference vanishes. In the subsequent separation process, external capacitors are switched to the series-connected again, causing the charges to flow back from TENG to external capacitors and forming a charge circulation loop. After a certain period of fast charge accumulation, surface charges will reach a high equilibrium state, which can be expressed as Equation (1) in the ideal case (no leakage of charges)

$$Q_{n+1} = Q_2 \left(1 + \frac{C}{2C_0 + C}\right)^{n-1} \quad (n \geq 2) \quad (1)$$

where Q is the amounts of charges of TENG, n is the number of times of contact-separation movement, C is the capacitance of TENG, and C_0 is the capacitance of capacitors in circuit. It can be found that the charges increase exponentially in the ideal case, that is, fast charge accumulation is realized by the self-charge excitation. The principle of fast charge accumulation is elaborated in Note S1 and Figure S1, Supporting Information.

On the other hands, the capacitance of TENG determines the maximum charge quantity which will be stored in TENG. Based on the parallel plate capacitor model, the capacitance value of TENG can be obtained. When the friction layer is in full contact, the capacitance of TENG can be described by Equation (2)

$$C = \frac{\epsilon_0 \epsilon_r S}{d} \quad (2)$$

where ϵ_0 is the vacuum dielectric constant, d and ϵ_r are thickness and relative permittivity of the dielectric material, respectively, and S is the area of the electrode. Meanwhile, the charge density of TENG can be expressed as Equation (3)

$$\sigma = \frac{\epsilon_0 \epsilon_r V}{d} \quad (3)$$

where V is the excitation voltage applied to TENG. The detailed derivation procedure and theoretical model are presented in Note S2 and Figure S2, Supporting Information.

According to the above analysis, manipulating the relative permittivity and thickness of the dielectric layer is greatly advantageous for the surface charges to reach a high equilibrium state. Thus, three materials, 25 μm poly(vinylidene fluoride) (PVDF) film, 8 μm Kapton film, and 9 μm poly(vinylidene fluoride-trifluoroethylene) (P(VDF-TrFE)) film (the scanning electron microscopy images of cross-sectional view are exhibited in Figure S3, Supporting Information), are used as dielectric layer. Their relative permittivity is 11.1, 7.5, and 3.7, respectively, as shown in Figure 1d (dielectric loss curves are shown in Figure S4, Supporting Information). Figure 1e exhibits the charge density and current density of TENG with different dielectric layers. The charge density of TENG is about

1.08 mC m^{-2} by using the PVDF film with high relative permittivity and large thickness. However, when the low relative permittivity film (e.g., Kapton) is utilized as dielectric layer, the charge density can also reach 1.00 mC m^{-2} owing to its small thickness (8 μm), which is one-third of the thickness of PVDF film (25 μm). The results demonstrate that high relative permittivity is also favorable to boost the charge density. When P(VDF-TrFE) with smaller thickness and higher relative permittivity is used as the dielectric layer, the charge density can be further enhanced to 2.20 mC m^{-2} , which is almost doubled. In addition, we have excluded the influence of piezoelectric effect of P(VDF-TrFE) film (more details are shown in Note S3, Supporting Information). The great improvement of output performance by utilizing P(VDF-TrFE) fully demonstrates the effectiveness of optimizing the relative permittivity of the dielectric layer. More importantly, the contact efficiency is 82% when using P(VDF-TrFE) film (Note S4, Supporting Information), higher than that of 4 μm PEI film (54.98%), thus avoiding the decrease of contact efficiency caused by reducing the thickness of dielectric film.^[30] Thus, the research method in this work not only achieves high charge density, but also opens up a new way for in-depth exploration of the output limit.

2.2. Output Performance of TENG via Fast Charge Accumulation

The excitation voltage of charge excitation TENG is determined by the number of VMC unit, namely N . In order to better understand the specific impact of excitation voltage on the equilibrium state, we measured the output performance of TENG combined with N -order VMC (circuit diagram is shown in Figure 2a, where $N = 2, 3, 4, 5$). The corresponding photographs of two parts of the self-charge excitation system are shown in Figure S5, Supporting Information. Despite the initial charge density of TENG is merely 0.11 mC m^{-2} , the output performance can be significantly improved when TENG is integrated with VMC units, as shown in Figure 2b. However, with a continuous increase of N , the charge density slightly increases from 1.08 mC m^{-2} ($N = 3$) to 1.20 mC m^{-2} ($N = 4$) and 1.25 mC m^{-2} ($N = 5$). The current density and voltage are shown in Figure 2c and Figure S6, Supporting Information. Actually, the electronic components in the circuit are equivalent to the external loads of TENG, which will consume some of the surface charges. The inevitable energy loss and finite output of TENG prevent the voltage across VMC from increasing linearly with the increase of N . Apart from this, the enhanced voltage across the TENG will increase the leakage current in the dielectric layer, which will augment the surface charge decay, as the decay curve shown in Figure 1a (ii). When the supplementary charges and the leaking charges are balanced, the charge density will reach saturation. Consequently, we prefer to choosing $N = 3$ for the following measurements due to its simpler structure of the device. In addition, the measurement results under different N are summarized in Table S1, Supporting Information. By the way, when utilizing Kapton and P(VDF-TrFE), the output performance of TENG combined with different VMC units is also measured, which exhibits the same growth trend, as demonstrated in Figures S7 and S8, Supporting Information, respectively.

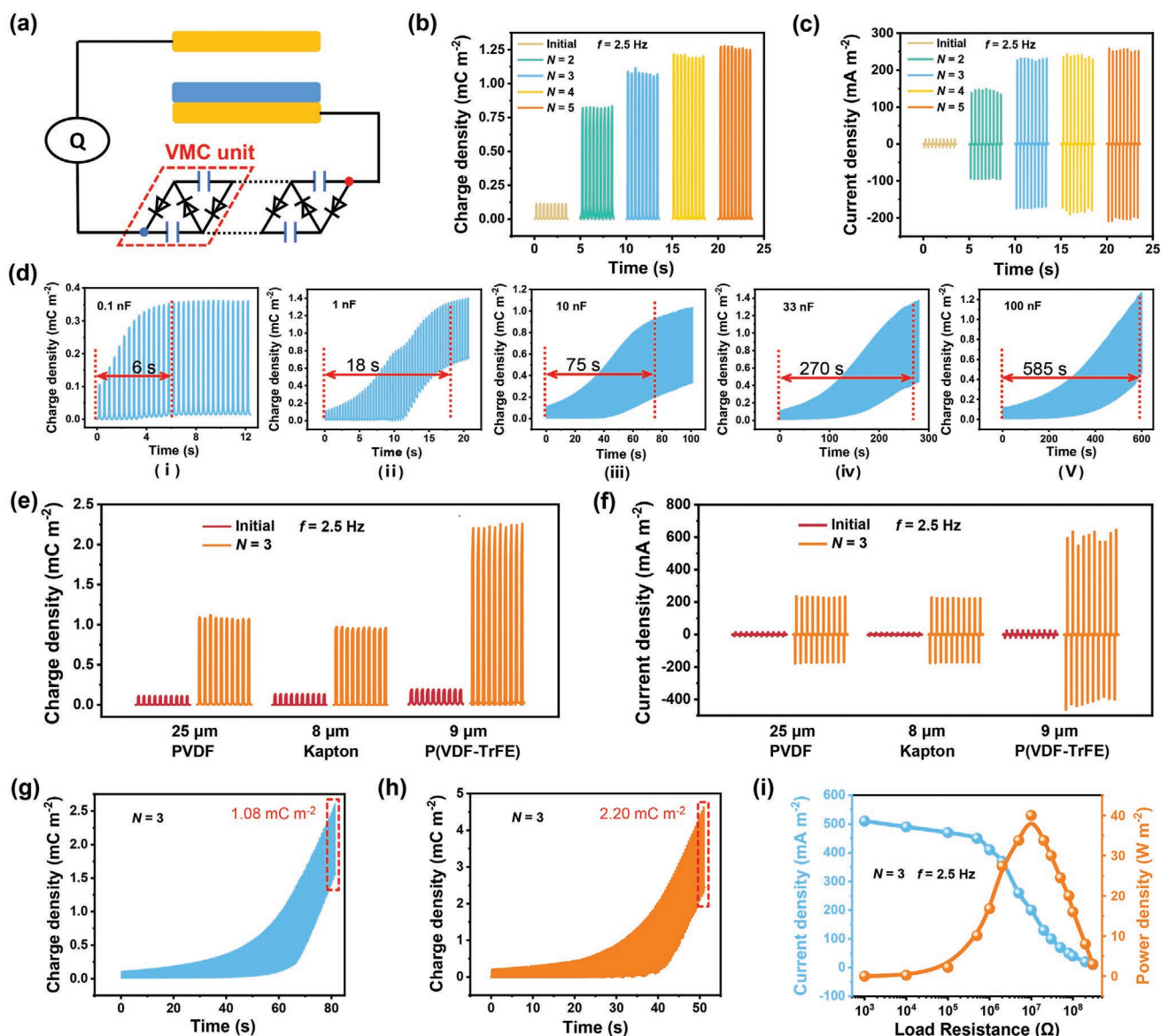


Figure 2. Output performance of TENG via fast charge accumulation. a) Simplified circuit diagram of self-charge excitation TENG with N -order VMC, in which $N = 2, 3, 4, 5$. b) Charge density and c) current density of TENG integrated with different VMC unit (dielectric layer: PVDF, operation frequency: 2.5 Hz). d) Charge accumulation time under different capacitance value of capacitors in circuit. e) Charge density and f) current density of TENG with three different dielectric materials under initial state and $N = 3$. g) Charge accumulation process with PVDF under $N = 3$. h) Charge accumulation process with P(VDF-TrFE) under $N = 3$. i) Current density and power density with P(VDF-TrFE) under $N = 3$.

According to Equation (1), the capacitance value of external capacitors also makes a big difference to the process of charge accumulation. Under different capacitance values (0.1, 1, 10, 33, and 100 nF, respectively), complete charge accumulation curves are shown in Figure 2d, respectively. In addition, comparison results are shown in Figure S9 and Table S2, Supporting Information. When using 0.1 nF capacitors, saturated charge density is 0.35 mC m^{-2} and the charge accumulation time is merely 6 s. As the capacitance value increases, the output charge density will also increase. Nevertheless, charge accumulation time shows an evident prolongation (Figure 2d), that is, charge accumulation speed decreases significantly. In brief, when the capacitance value is too small, the charges fed

back to TENG are insufficient to reach a high equilibrium state. On the contrary, when the capacitance value is too large, the charge accumulation speed will decrease, needing a longer time to reach the equilibrium state.

The output performance of the charge excitation TENG with three different dielectric layers is studied at 2.5 Hz. All of them have reached a high equilibrium state compared with the low equilibrium state of initial output. The corresponding charge density and current density are shown in Figure 2e,f, where the initial charge density of TENG with PVDF, Kapton and P(VDF-TrFE) is 0.11, 0.13, and 0.20 mC m^{-2} due to their different electronegativity. When charge accumulation speed increased, the charge density can be greatly enhanced, i.e.,

1.08, 1.00, and 2.20 mC m⁻² (the theoretical maximum charge density^[31] on P(VDF-TrFE) is 2.55 mC m⁻², as calculated in Note S5, Supporting Information, which is higher than the actual value due to incomplete contact between friction layers). Compared to the initial value, the charge density is increased by 8.8, 6.7, and 10.0 times, respectively, which means that the output performance is significantly improved and has little to do with the electrification ability of the friction materials in the case of using self-charge excitation. In addition, due to the high initial charge density and high relative permittivity of P(VDF-TrFE), its charge accumulation time is shorter than that of the other two despite its largest charge density, as summarized in Table S3, Supporting Information. When using PVDF and P(VDF-TrFE) films, complete charge accumulation curves are presented in Figure 2g,h, from which we can find that the surface charges increase exponentially at the beginning and then reach the high equilibrium state rapidly. Additionally, the baseline will rise in the late test period due to the air breakdown effect and leakage current in dielectric film (more details are shown in Note S6, Supporting Information). The current density and output power density by using P(VDF-TrFE) are shown in Figure 2i, where the load resistance varies from 1 KΩ to 300 MΩ. Maximum power density is 40.0 W m⁻² with a resistance of 10 MΩ at an operating frequency of 2.5 Hz, reaching 16 W m⁻² Hz⁻¹. Meanwhile, the current density and output power density by using PVDF under different resistance are shown in Figure S10, Supporting Information.

2.3. High Equilibrium State in High Humidity Environment

For a common TENG device, previous studies have demonstrated that the output performance generally degrades sharply with an increase of relative humidity in atmosphere.^[32] Based on the PVDF film, the output performance of TENG is measured under various relative humidity conditions (Figure 3a). As the relative humidity increases from 30% to 90%, the initial output performance of TENG declines sharply while the charge density under $N = 3$ still maintains a high value (0.90 mC m⁻² in 90% relative humidity). The corresponding current density and voltage are shown in Figure 3b and Figure S11a, Supporting Information. As we know, TENG is based on the coupling of triboelectrification effect and electrostatic induction effect, once water molecules are adsorbed on the surface of frictional layer, it will inevitably affect the process of charge generation.^[33] Therefore, with the increase of relative humidity, the more water molecules are absorbed on the surface of the PVDF film, the more surface triboelectric charges are dissipated. When the charge decay speed is greater than the charge accumulation speed, the charge density decreases gradually and reaches a low equilibrium state eventually. The initial charge density of TENG decreases from 0.11 to 0.025 mC m⁻² (≈78% loss) when relative humidity increasing from 30% to 90%. As for charge density under $N = 3$, it also presents a decreasing trend with the increase of relative humidity. Differently, the charge density only decreases from 1.12 to 0.9 mC m⁻² based on PVDF, implying a loss as low as 20% compared to the output under 30% relative humidity (Figure 3a). A conspicuous difference in output performance suggests that TENG with fast

charge accumulation can maintain its high equilibrium state even under high humidity environment. Different from the common TENG, the charge accumulation speed is still greater than the charge decay speed owing to fast charge accumulation strategy, so the surface charges still can be maintained at a high equilibrium state under a high relative humidity environment.

The difference between high and low equilibrium state is more obvious when using P(VDF-TrFE) in humidity environment, as demonstrated in Figure 3c,d. Since the dielectric film is thinner, its charge accumulation process is more susceptible to the influence of relative humidity. Even if relative humidity only increases to 45%, the output performance of TENG will drop dramatically, indicating a rapid charge decay. However, thanks to the fast charge accumulation, the surface charges still remain a high equilibrium state under $N = 3$, generating a high output performance. When the relative humidity is up to 90%, the common TENG only has a weak output signal of about 0.005 mC m⁻² while the charge density under $N = 3$ reaches up to 1.3 mC m⁻², so the charge density of the latter is almost 260 times that of the former (details of the voltage for both are shown in Figure S11b, Supporting Information). The above content not only elaborates the influence of humidity on equilibrium state, but also provides an effective method for achieving high output performance in high humidity environment.

With the operation frequency varying from 1 to 4 Hz, the charge density has barely dropped regardless of using PVDF or P(VDF-TrFE), as shown in Figure 3e. Additionally, the current density of both TENG is shown in Figure 3f, reaching the maximum of 540 and 200 mA m⁻² at 4 Hz, respectively. The voltage of TENG with P(VDF-TrFE) at different driving frequencies is exhibited in Figure S12, Supporting Information. All the charge density, current density, and voltage under different frequencies are measured in the ambient environment with relative humidity in the range of 30–40%.

2.4. Demonstrations of TENG to Drive Devices

Since there is a quadratic relation between the output power density and charge density, the high equilibrium state of surface charges can greatly enhance the output performance for various practical applications. In order to demonstrate the practicality, TENG with fast charge accumulation is used to power various electronic devices with an energy storage unit at 2.5 Hz. The circuit diagram of the system is depicted in Figure 4a. Charging curves of capacitors with different capacitance of 0.47, 1.00, and 2.20 μF are shown in Figure 4b. With the assistance of rectifier, two TENG devices in parallel can charge the 0.47, 1.00, and 2.20 μF capacitor to 40 V within 15, 33, and 83 s, respectively. In addition, the charging rate is 1.25, 1.18, and 1.06 μC s⁻¹ for charging the 0.47, 1.00, and 2.20 μF capacitor, respectively, demonstrating the advantage of the high charge density. As a more intuitive presentation in Figure 4c and Movie S1, Supporting Information, multiple blue LEDs connected in series can be lighted up even in a weak light circumstance. Apart from this, a digital watch also can be driven normally by the high-output TENG with a capacitor of 4.70 μF, as shown in Figure 4d and Movie S2, Supporting Information. Last but not least, stability test is conducted as illustrated in Figure 4e. After

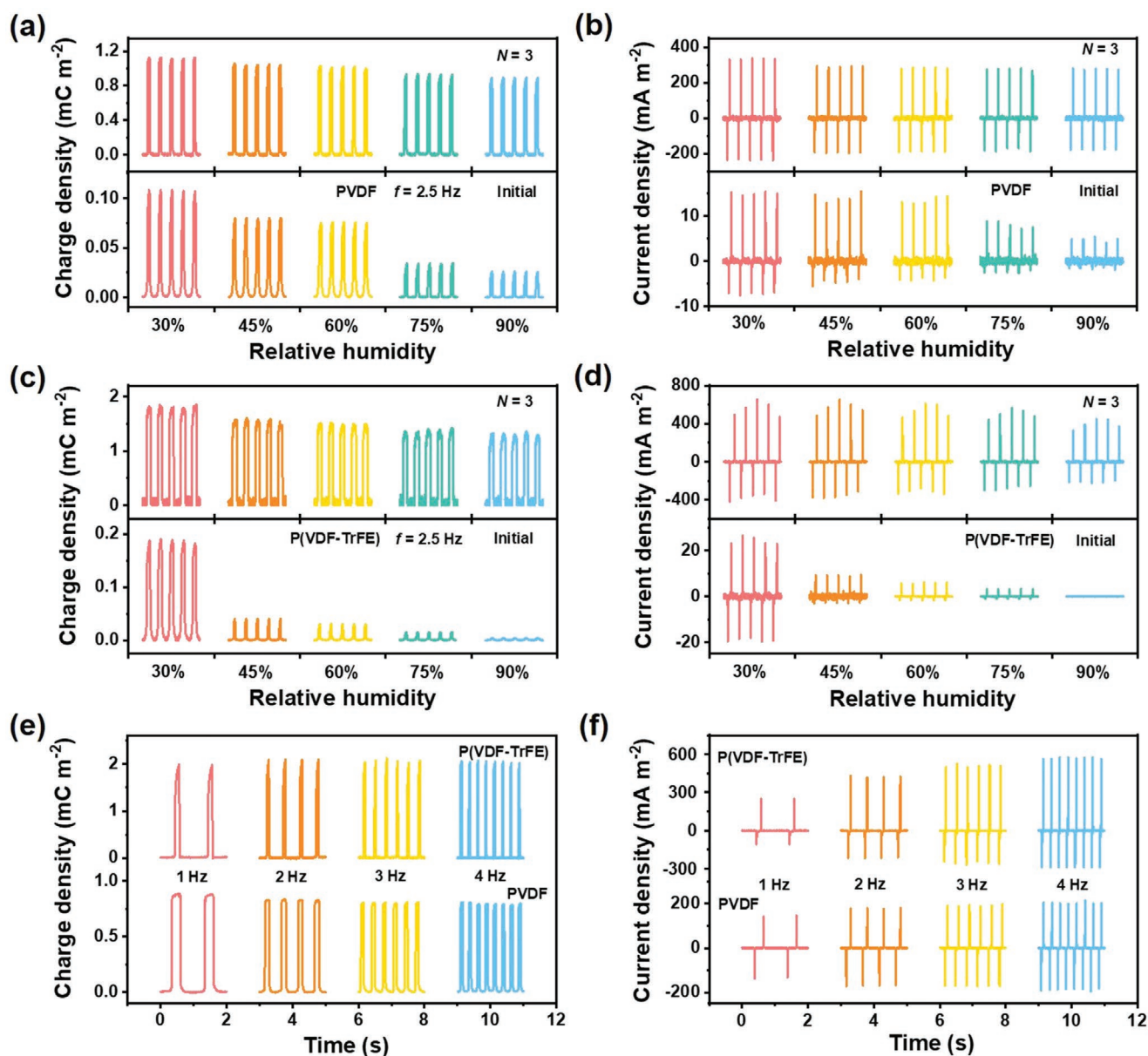


Figure 3. Equilibrium state under high ambient humidity. a) Charge density and b) current density of TENG with PVDF under initial state and $N = 3$ when changing ambient humidity. c) Charge density and d) current density with P(VDF-TrFE) under initial state and $N = 3$ when changing ambient humidity. e) Charge density and f) current density of TENG with PVDF and P(VDF-TrFE) under various operation frequency ($N = 3$).

54 000 operation cycles, the charge density has hardly degraded, indicating a good stability.

3. Conclusions

In summary, it has been demonstrated that using fast charge accumulation process on dielectric material with high relative permittivity is an effective approach to achieve high equilibrium state of surface charges and high output performance of TENG. Compared with the limited surface charges generated by triboelectrification of common TENG, fast charge accumulation can break through the limitation of triboelectrification

on surface charge density, which is also conducive to broaden the materials selection range of TENG. Therefore, benefit from the high relative permittivity of P(VDF-TrFE) together with fast charge accumulation, surface charge density reaches 2.20 mC m^{-2} , while the contact efficiency can be increased to 82%. In addition, it is expected to further raise the equilibrium state of surface charges through using dielectric materials with appropriate thickness, higher relative permittivity, and low leakage current. Besides, we also demonstrate that fast charge accumulation is greatly advantageous for boosting output performance under high humidity environment, which provides an instructive method for how to maintain the output performance of TENG working in high humidity environments. This work not

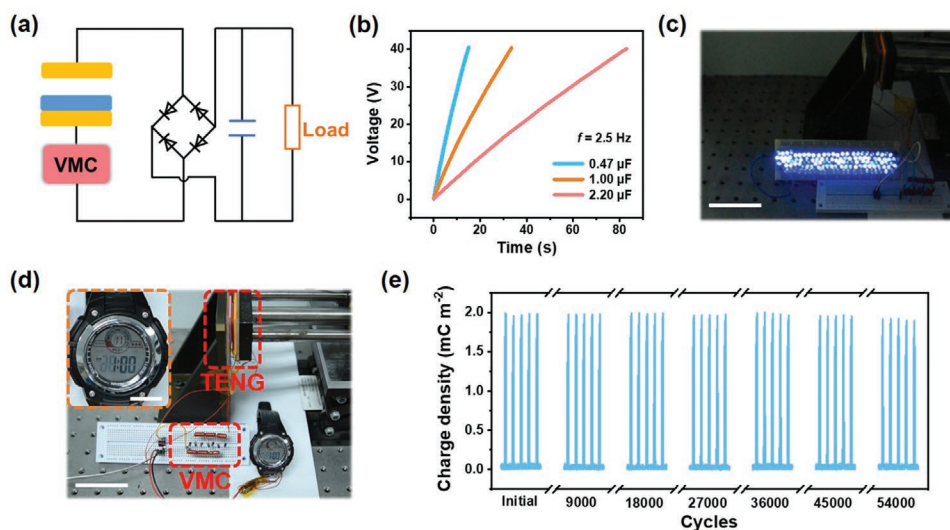


Figure 4. Demonstrations of the high equilibrium state TENG to drive devices. a) Circuit diagram of TENG with an energy storage unit for powering electronics. b) Charging curves of different capacitors at 2.5 Hz by two TENG devices in parallel. c) LEDs lighted up by high equilibrium state TENG (scale bar, 5 cm). d) A digital watch driven by high equilibrium state TENG (scale bar, 5 cm; scale bar of insert, 1 cm). e) Stability test of high equilibrium state TENG with 54 000 operation cycles.

only offers an insight into the charge accumulation and equilibrium state by the charge excitation tool, but also presents a new approach for further optimization of the output performance of TENG.

4. Experimental Section

Fabrication of the Charge Excitation TENG: As is illustrated in Figure 1b, the charge excitation TENG is mainly composed of acrylic sheets, foam, silicone layer, two Cu electrodes, and a dielectric layer, where the foam and silicone layer together form a buffer layer. The fabrication process is as follows. First, the acrylic sheet was cut by laser cutter with dimensions of $45 \times 45 \times 3$ mm and a 2 mm foam with the same size was adhered to the surface of acrylic sheet. Then, the silicone layer with dimensions of $30 \times 30 \times 1$ mm (Ecoflex 10) was adhered to the upper surface of the foam, which was prepared by mixing the base and the curing agent in a 1:1 weight ratio and curing under 60 °C for at least 1 h. Afterwards, a chamfered 2 mm, 20×20 mm Cu electrode was sputtered on the dielectric film; one side of 30×30 mm dielectric films (25 μm PVDF, 8 μm Kapton, and 9 μm P(VDF-TrFE)) with the electrode was attached to the silicone layer. As for another electrode, a circular electrode with an area of 1 cm² was sputtered on the Kapton film; one side of 30×30 mm Kapton film without the electrode was adhered to the silicone layer. For the VMC, the maximum working voltage of rectifier is 50 V; the rated voltage value of different capacitors is 630 V and the capacitance of different capacitors is 0.1, 1, 10, 33, and 100 nF, respectively.

Measurement and Characterization: The periodic contact-separation process of TENG was driven by a linear motor (TSMV120-1S). Short-circuit current and transferred charges of TENG were measured by a programmable electrometer (Keithley model 6514). The voltage of initial was also measured by electrometer (Keithley model 6514) under different relative humidity. Meanwhile, other voltage curves in this work were measured by an oscilloscope (MDO 3024). Relative humidity of environment is controlled by high- and low-temperature alternating damp heat test chamber (DHTM-50-40-AR-SD). The microstructures of films were conducted by a cold field emission scanning electron microscope (Hitachi SU8200). The relative permittivity of three dielectric materials was tested by an LCR measurement instrument (E4980AL-100).

Supporting Information

Supporting Information is available from the Wiley Online Library or from the author.

Acknowledgements

Y.L., Z.Z., and L.L. contributed equally to this work. This research was supported by the National Key R&D Project from Minister of Science and Technology (2016YFA0202701), National Natural Science Foundation of China (grant no. 61774016, 51432005, 5151101243, and 51561145021), and China Postdoctoral Science Foundation (2019TQ0361 and 2020M672962).

Conflict of Interest

The authors declare no conflict of interest.

Data Availability Statement

The data that support the findings of this study are available in the supplementary material of this article.

Keywords

fast charge accumulation, high equilibrium state, surface charge density

Received: January 7, 2021
Revised: February 10, 2021
Published online: March 4, 2021

- [1] S. Chu, A. Majumdar, *Nature* **2012**, *488*, 294.
- [2] F.-R. Fan, Z.-Q. Tian, Z. L. Wang, *Nano Energy* **2012**, *1*, 328.
- [3] J. Bae, J. Lee, S. Kim, J. Ha, B. S. Lee, Y. Park, C. Choong, J. B. Kim, Z. L. Wang, H. Y. Kim, J. J. Park, U. I. Chung, *Nat. Commun.* **2014**, *5*, 4929.

- [4] J. Wang, S. Li, F. Yi, Y. Zi, J. Lin, X. Wang, Y. Xu, Z. L. Wang, *Nat. Commun.* **2016**, *7*, 12744.
- [5] Z. L. Wang, *Adv. Energy Mater.* **2020**, *10*, 2000137.
- [6] Z. L. Wang, J. Chen, L. Lin, *Energy Environ. Sci.* **2015**, *8*, 2250.
- [7] Z. L. Wang, A. C. Wang, *Mater. Today* **2019**, *30*, 34.
- [8] C. Wu, A. C. Wang, W. Ding, H. Guo, Z. L. Wang, *Adv. Energy Mater.* **2019**, *9*, 1802906.
- [9] L. Zhou, D. Liu, J. Wang, Z. L. Wang, *Friction* **2020**, *8*, 481.
- [10] J. Cheng, W. Ding, Y. Zi, Y. Lu, L. Ji, F. Liu, C. Wu, Z. L. Wang, *Nat. Commun.* **2018**, *9*, 3733.
- [11] P. Cheng, H. Guo, Z. Wen, C. Zhang, X. Yin, X. Li, D. Liu, W. Song, X. Sun, J. Wang, Z. L. Wang, *Nano Energy* **2019**, *57*, 432.
- [12] H. Guo, X. Pu, J. Chen, Y. Meng, M. Yeh, G. Liu, Q. Tang, B. Chen, D. Liu, S. Qi, C. Wu, C. Hu, J. Wang, Z. L. Wang, *Sci. Rob.* **2018**, *3*, eaat2516.
- [13] R. Hinchet, H. J. Yoon, H. Ryu, M. K. Kim, E. K. Choi, D. S. Kim, S. W. Kim, *Science* **2019**, *365*, 491.
- [14] X. Liang, T. Jiang, G. Liu, Y. Feng, C. Zhang, Z. L. Wang, *Energy Environ. Sci.* **2020**, *13*, 277.
- [15] J. Luo, Z. Wang, L. Xu, A. C. Wang, K. Han, T. Jiang, Q. Lai, Y. Bai, W. Tang, F. R. Fan, Z. L. Wang, *Nat. Commun.* **2019**, *10*, 5147.
- [16] X. Peng, K. Dong, C. Ye, Y. Jiang, S. Zhai, R. Cheng, D. Liu, X. Gao, J. Wang, Z. L. Wang, *Sci. Adv.* **2020**, *6*, eaba9624.
- [17] H. Guo, J. Chen, L. Wang, A. C. Wang, Y. Li, C. An, J.-H. He, C. Hu, V. K. S. Hsiao, Z. L. Wang, *Nat. Sustainability* **2021**, *4*, 147.
- [18] H. Zhang, F. Marty, X. Xia, Y. Zi, T. Bourouina, D. Galayko, P. Basset, *Nat. Commun.* **2020**, *11*, 3221.
- [19] Z. Wang, W. Liu, W. He, H. Guo, L. Long, Y. Xi, X. Wang, A. Liu, C. Hu, *Joule* **2021**, *5*, 441.
- [20] Y. Zi, S. Niu, J. Wang, Z. Wen, W. Tang, Z. L. Wang, *Nat. Commun.* **2015**, *6*, 8376.
- [21] N. Cui, L. Gu, Y. Lei, J. Liu, Y. Qin, X. Ma, Y. Hao, Z. L. Wang, *ACS Nano* **2016**, *10*, 6131.
- [22] S. Wang, Y. Xie, S. Niu, L. Lin, C. Liu, Y. S. Zhou, Z. L. Wang, *Adv. Mater.* **2014**, *26*, 6720.
- [23] X. Cui, Y. Zhang, *Nano Select* **2020**, *1*, 461.
- [24] X. Cui, Y. Zhang, G. Hu, L. Zhang, Y. Zhang, *Nano Energy* **2020**, *70*, 104513.
- [25] J. Wang, C. Wu, Y. Dai, Z. Zhao, A. Wang, T. Zhang, Z. L. Wang, *Nat. Commun.* **2017**, *8*, 88.
- [26] J. Fu, G. Xu, C. Li, X. Xia, D. Guan, J. Li, Z. Huang, Y. Zi, *Adv. Sci.* **2020**, *7*, 2001757.
- [27] L. Cheng, Q. Xu, Y. Zheng, X. Jia, Y. Qin, *Nat. Commun.* **2018**, *9*, 3773.
- [28] H. Wang, L. Xu, Y. Bai, Z. L. Wang, *Nat. Commun.* **2020**, *11*, 4203.
- [29] W. Liu, Z. Wang, G. Wang, G. Liu, J. Chen, X. Pu, Y. Xi, X. Wang, H. Guo, C. Hu, Z. L. Wang, *Nat. Commun.* **2019**, *10*, 1426.
- [30] Y. Liu, W. Liu, Z. Wang, W. He, Q. Tang, Y. Xi, X. Wang, H. Guo, C. Hu, *Nat. Commun.* **2020**, *11*, 1599.
- [31] C. Zhang, L. Zhou, P. Cheng, X. Yin, D. Liu, X. Li, H. Guo, Z. L. Wang, J. Wang, *Appl. Mater. Today* **2020**, *18*, 100496.
- [32] L. Li, X. Wang, P. Zhu, H. Li, F. Wang, J. Wu, *Nano Energy* **2020**, *70*, 104476.
- [33] R. Wen, J. Guo, A. Yu, J. Zhai, Z. L. Wang, *Adv. Funct. Mater.* **2019**, *29*, 1807655.